OH in detrital quartz grains as tool for provenance analysis: case studies on various settings from Cambrian to Recent

Roland Stalder [a,*], Hilmar von Eynatten [b], Julian Costamoling [a], Alexander Potrafke [a], István Dunkl [b], Guido Meinhold [b,c]

[a] Institut für Mineralogie und Petrographie, Universität Innsbruck, Innrain 52f, A-6020 Innsbruck, Austria

[b] Geowissenschaftliches Zentrum der Universität Göttingen, Goldschmidtstraße 3, D-37077 Göttingen, Germany

[c] School of Geography, Geology and the Environment, Keele University, Staffordshire, ST5 5BG, Keele, UK

* Corresponding author.

E-mail address: roland.stalder@uibk.ac.at (R. Stalder).

Abstract

Detrital quartz grains from Paleozoic and Mesozoic sandstones from North Africa and central Europe, respectively, and from recent siliciclastic sediments of the Elbe River from Germany were analysed by IR spectroscopy with respect to their OH defect content. Sample sets were carefully chosen to cover different stratigraphic units from different localities and according to previous findings that indicate a significant change in the source region in the respective sedimentary system. The validity of the new method is compared to heavy mineral and zircon age spectra analysis from previous studies. Results reveal that the OH defect inventory in quartz shows in all investigated sedimentary successions significant internal variations from sample to sample and thus may be used as a tool to identify changes in the source region. The degree of changes observed with the new method does not necessarily reflect the magnitude in differences observed by other methods (such as heavy minerals and/or zircon age spectra), underlining the potential as complementary tool for provenance analysis. The new tool is also tested to estimate mixing proportions between the Variscan and the Scandinavian signal in the Elbe River, resulting in a surprisingly high contribution of the Nordic source.

Keywords: Quartz; OH defects; IR spectroscopy; provenance

1. Introduction

Quartz belongs to the most abundant minerals in the Earth's crust and is a major constituent of clastic sediments. Because of its high resistance against mechanical and chemical weathering and its stability up to low-grade metamorphic condition, individual grains often survive erosion and transport over long distances and even postdepositional diagenetic overprint up to low-grade metamorphism. Depending on the initial crystallisation conditions (often inherited from the parent igneous systems), quartz incorporates different amounts and

types of hydrous defects (OH defects), where Si^{4+} is replaced by metal cations and protons (Bambauer, 1961; Kats, 1962; Aines and Rossman, 1984; Müller and Koch-Müller, 2009; Stalder and Konzett, 2012) that are very sensitive towards absorption of IR radiation. Hydrous defects are preserved over geological time scales at diagenetic conditions (Stalder, 2014) and are not totally reset until 300–400°C (Stalder et al., 2017), and therefore either serve as valuable archive for initial crystallisation conditions (OH defects still present) or indicate metamorphic overprint (OH defects largely destroyed). Compared to the most common characterisation tools of quartz in sediments – cathodoluminescence emission spectra (Matter and Ramsayer, 1985; Götze et al., 2001; Augustsson and Reker, 2012) and trace element analysis by laser ablation-ICP-MS (Müller and Knies, 2013; Ackerson et al., 2015) – IR spectroscopy adds additional characteristics to discriminate detrital quartz: (1) major defect-types give rise to energy specific IR absorption bands without significant overlap (Kats, 1962; Aines and Rossman, 1984), (2) IR absorption bands are chemically well understood and can be linked to a specific type of defect (Stalder and Konzett, 2012; Baron et al., 2015; Frigo et al., 2016), and (3) OH defect concentrations in nominally anhydrous minerals can be quantified down to the ppm level (Aines et al., 1984; Libowitzky and Rossman, 1997).

Quartz from igneous rocks generally contains significantly higher amounts of OH defects than quartz annealed under metamorphic conditions (Müller and Koch-Müller, 2009; Stalder and Neuser, 2013). A rough distinction between granitic, pegmatitic and metamorphic sources is possible, in that pristine granitic quartz generally exhibits OH defects, late stage igneous quartz (pegmatitic, hydrothermal) shows increased content in Li- and/or B-specific OH defect, and metamorphic quartz is poor in OH. It was also suggested that very old igneous sources are often poor in OH (Stalder et al., 2017), probably because they nearly always experienced at least low-grade metamorphism once in their geological past.

In this study, it is tested whether the change in source material in sedimentary systems is visible in the OH defect inventory in detrital quartz grains and in how far these differences can be applied to provenance analysis. For this purpose, three sets of two samples were chosen (Table 1), for which a substantial change with respect to provenance is documented by other methods such as heavy mineral analysis and zircon U–Pb age determination.

2. Samples and methods

2.1.Samples

Three case studies were performed representing siliciclastic sedimentary successions from the Lower Paleozoic of southern Libya and the Lower Mesozoic of southern Germany, and modern sediment from a major river system in Germany. From each of the three sample sets detrital quartz grains from two different stratigraphic units (in case of the Elbe River: different localities) were analysed by IR spectroscopy with respect to their OH defect content. Sample sets were carefully chosen according to previous findings that indicate changes in sediment provenance in the respective sedimentary system. Sample details are summarised in Table 1.

W5207 is a medium-grained quartz arenite from the Hasawnah Formation (Cambrian) of central Dor el Gussa (DEG), Libya. The Hasawnah Formation represents a braided fluvial to shallow marine environment (Čepak, 1980; Le Heron et al., 2013). Heavy minerals are strongly dominated by zircon (90%). About 80% of the zircon grains exhibit Pan-African ages (<1000 Ma, ~70% are between 550–700 Ma), ~15% are 1000–2500 Ma old, and only 3% are Archean. A more detailed documentation can be found in Meinhold et al. (2011) and Morton et al. (2011).

H6048 is a medium-grained quartz arenite from the Hawaz Formation (Middle Ordovician) of central Dor el Gussa (DEG), Libya. The sample was deposited in a near-shore platform setting (Ramos et al., 2006; Le Heron et al., 2013). The heavy mineral spectrum is similar to sample W5207, but only ~50% of the zircon grains exhibit Pan-African ages (<1000 Ma, ~25% are between 550–700 Ma), roughly 40% are 1000–2500 Ma old, and ~11% are of Archean age (Meinhold et al., 2011).

EY54-18 is a fine- to medium-grained quartz-rich sandstone (lithic subarkose) from a borehole at Ensingen/Germany, which represents the Bausandstein unit of the Lower Triassic Lower to Middle Buntsandstein (Simon et al., 2013). The Buntsandstein was deposited in a fluvial to lacustrine continental red bed setting in the Central European Basin related to the breakup of Pangea (e.g., Bourquin et al., 2006). The heavy mineral fraction is dominated by the ultrastable minerals zircon, tourmaline and rutile, complemented by apatite, while zircon U–Pb age spectra are dominated by Variscan, Caledonian and Cadomian age components (Schade, 2018).

EY54-11 is a fine-grained quartz-rich micaceous sandstone (lithic subarkose) derived from a borehole at Ensingen/Germany, which represents the Plattensandstein unit from the Lower Triassic Upper Buntsandstein (Simon et al., 2013). The heavy mineral fraction is, besides a high amount of barite, dominated by apatite, zircon, tourmaline and rutile (Schade, 2018). Similarly, zircon ages resemble the data from the Lower to Middle Buntsandstein sample EY54-18. This observation is in contrast to significant changes in facies and texture generally described at the transition from the Middle to the Upper Buntsandstein (e.g., Bourquin et al., 2006, Lepper et al., 2013).

EY49-29 is a quartz-rich sand from the Elbe River close to Torgau/Germany, about 100 km downstream from Dresden. The heavy mineral composition is characterised by high proportions of pyroxene and amphibole, and zircon U–Pb ages reveal a strong Variscan age component (360 – 300 Ma; Aschoff, 2017), indicating a predominant provenance from primary and recycled sources of the Bohemian massif (e.g., Erzgebirge).

EY53-23 is a quartz-rich sand from the Elbe River close to Geesthacht/Germany, about 25 km upstream from Hamburg. The heavy mineral composition is characterised by high proportions of garnet and zircon, and zircon U–Pb ages reveal a major Grenvillian (Sveconorwegian) age component (approximately 1200 to 950 Ma) followed by Paleoproterozoic ages and minor Variscan ages (Führing, 2017). This indicates a strong downstream admixture (as compared to sample EY49-29) of Scandinavian sources, most likely through extensive recycling of Pleistocene glacial deposits from the lowlands of northern Germany.

2.2.Sample preparation and infrared (IR) spectroscopy

Quartz grains in the sandstone samples (W5207, H6048, EY54-11, EY54-18) were prepared as double-polished thick sections (120 µm), and the sand material (EY49-29, EY53-23) was prepared as grain mounts with a thickness of 120 µm from the 250–500 µm fraction. In order to remove the glass slides and the resin used for preparation, all mounts and thick sections were rinsed for several hours in acetone.

IR spectra were recorded at room temperature in transmission mode using a Bruker Vertex 70 FTIR spectrometer, coupled to a Hyperion 3000 microscope equipped with a liquid nitrogen-cooled MCT-detector, a globar light source, a KBr beamsplitter and a wire-grid IR-polariser and two polarisers for visible light. Absorption bands of OH defects energetically

overlap with absorption bands from fluid inclusion that may be by far the most important repository of OH in quartz (Bambauer, 1961; Aines et al., 1984; Müller and Koch-Müller, 2009). However, in contrast to the isotropic signal of liquid water from the fluid inclusions, OH defects are strongly polarised perpendicular to the crystallographic c-axis (identical to the optical axis). In order to eliminate the molecular water signal from the OH defect signal, we followed the strategy described by Stalder and Konzett (2012) and Stalder and Neuser (2013), and performed polarised spectroscopic measurements on oriented grains. Specifically, crystal sections parallel to the c-axis are selected, and measurements $||n_o$ and $||n_e$ were performed. The pure OH defect signal was derived by subtracting the absorbances A of the two polarised measurements ($A||n_o$ - $A||n_e$). Appropriate crystal sections were selected based on their interference colour in visible light under crossed nicols under the FTIR microscope. Given the sample thickness (d) of 120 µm and the maximum birefringence (Δ) of 0.009, only grains with an interference colour close to red II (the theoretical value for our samples is $d \cdot \Delta$=1080 nm path difference, close to the 1100 nm for red II) were taken into consideration for IR measurements. As for practical reasons not every grain could be checked for perfect orientation by conoscopic illumination, it is estimated that all grains with a path difference down to 1030 nm (where red II starts to turn into orange) were considered for measurements. This deviation corresponds to a tilt angle of 12–13° from the perfect orientation (following the function $\Delta/\Delta_{max}=\cos^2\varphi$). Assuming random orientation, theoretically 7% of all grains fulfil this requirement (in uniaxial crystals the abundance $H(\Delta)$ is proportional to the square root of Δ and integration of this function between Δ/Δ_{max}=0.95 and 1 yields 0.07), which is in agreement to the practical observation that in a grain mount of 1000–2000 grains 100 grains could be measured. The error for the measured absorbance $A||n_e$ follows the same function as the deviation from interference colour ($A||n_e = \cos^2\varphi$), leading to a systematic error of $A||n_o$ - $A||n_e$ of 5% and values reported for OH contents may therefore be up to 5% too low (note that

A||n_o has no such systematic error as the refractive index n_o is exhibited in all sections in uniaxial crystals).

After selection of a suitable grain the optical polarisers were removed, the IR polariser was adjusted, and two measurements were performed with a spectral resolution of 2 cm^{-1} in the 550 to 7500 cm^{-1} range. No fitting procedure was applied to the observed absorption bands, instead the defect water content (expressed as wt ppm water) was derived by multiplying the absorbance for each measured channel with an individual extinction coefficient according to the calibration of Libowitzky and Rossman (1997). If necessary, a thickness correction (Stalder et al., 2017) according to the lattice overtones between 1200 and 2200 cm^{-1} was applied. Subtracted spectra (n_o-n_e) were normalised to thickness and corrected by a linear baseline between 3250 and 3610 cm^{-1}. In a few cases, when B-related OH absorption bands (occurring at 3595 cm^{-1} and exhibiting absorption ||n_o and ||n_e) were observed, spectra were corrected in the 3585–3605 cm^{-1} range, taking into account the total dipole intensity defined as 2o+e (Stalder and Neuser, 2013; Baron et al., 2015). For the used sample thickness the detection limit of OH (expressed as water equivalent) is around 1 wt ppm H_2O.

3. Results

The number of successfully measured grains and OH contents are given in Table 1. Samples within one case study or sedimentary succession show significant variations with respect to the OH defect inventory and the average OH content within one sample set spread by a factor of 1.5–2, which is clearly mirrored in the magnitude of the IR absorption bands (Fig. 1). All spectra are dominated by the absorption band at 3378 cm^{-1} caused by the Al-specific OH defect, followed by the Li-specific defect at 3470–3480 cm^{-1}, which is very minor in the Paleozoic samples from Libya (W5207, H6048), discernable in the Elbe River samples

(EY49-29, EY53-23) and very clear in the Lower Triassic sandstones from Germany (EY54-11, EY54-18). For better comparison of absorption band ratio of the two samples from each set, spectra with the lower absorbance were scaled (Fig. 1) to match the total absorbance of the sample with the stronger absorbance. After scaling, the spectra from both Elbe River samples are identical within error, but the other two sample sets show subtle differences with respect to the band ratio, where EY54-18 and H6048 have slightly higher ratios of Li- (at 3480 cm^{-1}) to Al-specific (at 3378 cm^{-1}) absorption bands than their counterparts in the same sedimentary succession.

The distribution of OH defect contents show significant differences within all three sample sets (Figs. 2, 3): (1) in the Paleozoic sandstones from Libya the OH rich fraction (15–40 wt ppm) is much more abundant in sample W5207 (Cambrian Hasawnah Formation) than in the Ordovician sample (H6048); (2) in the Lower Triassic sandstones from Germany the OH rich fraction (15–40 wt ppm) is much more abundant in sample EY54-18 (Lower to Middle Buntsandstein) than in the Upper Buntsandstein sample (EY54-11) and the OH poor fraction (<5 wt ppm) is much more abundant in the Upper Buntsandstein sample (EY54-11); (3) in the recent Elbe River sediment the downstream sample EY53-23 is strongly enriched in OH poor grains (<5 wt ppm) compared to the upstream sample EY49-29 (thereby all other classes appear less abundant).

Finally, it is worth noting that the average of all samples again clusters around 10 wt ppm, representing the global average of crustal quartz (Stalder, 2014).

4. Discussion

Spectral shapes and OH distributions can be used to evaluate possible scenarios that lead to the changes in OH inventory in quartz. Specifically, strong absorption bands at 3470–3480 cm^{-1} and 3595 cm^{-1} are linked to Li- and B-related OH defects (Müller and Koch-Müller,

2009; Baron et al., 2015; Frigo et al., 2016) and may hint to quartz from late stage igneous sources such as low-T hydrothermal and pegmatitic quartz (Stalder and Neuser, 2013). Based on these thoughts, data from the Elbe River samples are in accord with the interpretation that the detritus from the Bohemian massif (containing an average of 12 wt ppm defect water as observed in sample EY49-29) is mixed with reworked glacial deposits initially derived from the Scandinavian shield, which are generally very OH poor (Stalder et al., 2017). There are several ways to estimate the mixing ratio of both sources. If an average of 4 wt ppm defect water for the glacial deposits (corresponding to dune sands from the southern Baltic Sea, Stalder et al., 2017) is assumed and taking sample EY49-29 as "Bohemian endmember" the ratio of both sources is 1:1, resulting in an average of 8 wt ppm water, as observed in the Elbe River sample from Geesthacht (EY53-23). If we assume that the glacial source was virtually OH free, we get a mixing ratio Bohemian:Scandinavian source of 2:1. The latter interpretation is supported by the fact that the average IR spectra are identical after rescaling (Fig. 1), meaning that the Bohemian signal is just diluted by a zero-signal. A more sophisticated deconvolution of the OH defect distributions applying the algorithm of Dunkl and Székely (2002) yields three components for each of the two samples (Fig. 4): 0.6 ± 0.2 ppm (5%), 7.7 ± 4.8 ppm (66%) and 23.9 ± 8.5 ppm (29%) at Torgau (EY49-29), and 0.9 ± 1.1 ppm (39%), 4.6 ± 2.4 ppm (30%) and 18.2 ± 9.3 ppm (31%) at Geesthacht (EY53-23). Attributing only the <2 ppm components (i.e. virtually OH free) to the Scandinavian source would imply admixture of about 1/3 of such grains in the downstream sample at Geesthacht, supporting a mixing ratio Bohemian:Scandinavian source of approximately 2:1. Additional attribution of, at least, part of the 4.6 ± 2.4 ppm component in the Geesthacht sample to the Scandinavian source, which seems plausible according to previous results (Stalder et al., 2017), would push the ratio towards 1:1. These ratios suggest a smaller Scandinavian component compared to rough estimates based on the heavy mineral and zircon U–Pb data (Führing, 2017). In view of

the complex factors controlling heavy mineral assemblages and especially zircon age distributions (e.g., Garzanti et al., 2009; Malusa et al., 2016), mixing calculations based on a major sediment component like quartz may be more robust than those based on very small fractions of the detrital grains, particularly if the mixed sources have strongly different contents in accessory minerals.

Despite a well-documented general change in sedimentary facies, texture and composition in the Lower Triassic around the Middle to Upper Buntsandstein transition (e.g., Bourquin et al., 2006; Lepper et al., 2013; Meyerink et al., 2017) a significant difference in heavy minerals and/or zircon ages has not been detected between the two Buntsandstein samples EY54-18 and EY54-11. A fortiori, it is astonishing that the OH defect inventory between both samples shows very clear differences (Figs. 2, 3). The total average absorbance (Fig. 1) differs nearly by a factor of two and the IR spectra of the OH poorer, younger sample (EY54-11) has a lower ratio of Li- to Al-specific bands. The distribution suggests at least three different sources, one OH poor (only in EY54-11), one OH rich (only in EY54-18) and one common source (Fig. 5). A rough estimate of the relative proportions between these different sources is 1:1:2, respectively. The shift towards more OH poor sources along with relative increase of Al-specific OH defects for the younger Upper Buntsandstein sample most likely points to a higher proportion of metamorphic and/or deeper seated and/or older igneous rocks in the source area (Stalder et al., 2017).

Concerning the Paleozoic sandstones from Libya, the change towards gradual lower OH defect contents from the Cambrian (W5207) to the Ordovician (H6048) correlates well with the increase of 1-Ga-old zircons interpreted as detritus from the Transgondwana supermountain supplied via the Gondwana super-fan system (Meinhold et al., 2013) and older sources. However, the difference in OH is not as clear as expected from the change in zircon ages, suggesting that either (1) the older sources supplied (related to quartz) more heavy

minerals, (2) zircon became enriched relative to quartz during transport over long distances because of its higher hardness (3), the difference in OH in quartz of the older sources was not well pronounced.

In summary, results reveal that the OH defect inventory, expressed in the shape of the IR spectra, the average total absorbance and the distribution from grain to grain, offer many parameters to characterise sedimentary samples, and thus can be used as tool to identify and interpret changes in the source region. However, a strong change in OH defects within a given succession does not necessarily coincide with strong differences in heavy minerals and/or zircon age spectra, underlining the potential as new and complementary tool for provenance analysis.

5. Conclusions

(1) Siliciclastic samples show significant variations with respect to the OH defect inventory in quartz grains within a sedimentary succession or spatially evolving sedimentary systems and thus may be used as tool to identify changes in the source region.

(2) Changes in different samples from one succession may or may not reflect the differences in heavy minerals and/or zircon age spectra, underlining the potential as new and complementary tool for provenance analysis.

(3) OH defect distributions allow us to estimate mixing relations between different sources in modern river systems, which are based on major constituents such as quartz and may thus turn out to be more robust than estimates based on accessory minerals.

(4) Average IR spectra can be used to discriminate contributions of young igneous and old metamorphic overprinted material.

Acknowledgements

This work was supported by the Austrian Science Fund (FWF): P29145-N34. GM wishes to acknowledge the sponsors of the CASP Southern Libyan Basins Project for the requisite financial support for fieldwork, and the late Andrew G. Whitham (CASP) for the permission to use the Libya samples in this study. Many thanks to Manfred Martin and Edgar Nitsch (LGRB Baden Württemberg) for providing information and access to the drillcore Ensingen. Franz Gartner is thanked for preparing grain mounts and thick sections for IR spectroscopy measurements. Abhijit Basu and an anonymous reviewer are thanked for thorough and constructive reviews.

References

Ackerson, M.R., Tailby, N.D., Watson, E.B., 2015. Trace elements in quartz shed light on sediment provenance. Geochemisty Geophysics Geosystems 16, 1894-1904.

Aines, R.D., Kirby, S.H., Rossman, G.R., 1984. Hydrogen speciation in synthetic quartz. Physics and Chemistry of Minerals 11, 204-212.

Aines, R.D., Rossman, G.R., 1984. Water in minerals? A peak in the infrared. Journal of Geophysical Research 89, 4059-4071.

Aschoff, M., 2017. Modern sands from the German North Sea coast and the Elbe River – Scandinavian vs. Variscan provenance. Unpublished MSc-thesis, University of Göttingen, 90 pp.

Augustsson, C., Reker, A., 2012. Cathodoluminescence spectra of quartz as provenance indicators revisited. Journal of Sedimentary Research 82, 559-570.

Bambauer, H.U., 1961. Spurenelementgehalte und γ-Farbzentren in Quarzen aus Zerrklüften der Schweizer Alpen. Schweizerische Mineralogisch Petrographische Mitteilungen 41, 335-369. (in German with English abstract)

Baron, M.A., Stalder, R., Konzett, J., Hauzenberger, C.A., 2015. Formation conditions of quartz recorded by OH-point defects – experimental and analytical approach. Physics and Chemistry of Minerals 42, 53-62.

Bourquin, S., Peron, S., Durand, M., 2006. Lower Triassic sequence stratigraphy of the western part of the Germanic Basin (west of Black Forest): Fluvial system evolution through time and space. Sedimentary Geology 186, 187-211.

Čepak, P., 1980. The sedimentology and facies development of the Hasawnah Formation in Libya. In: Salem, M.J., Busrewil, M.T. (Eds.), The Geology of Libya. Academic Press, London, vol. 2, pp. 375-382.

Dunkl, I., Székely, B., 2002. Component analysis with visualization of fitting – PopShare, a Windows program for data analysis. *Goldschmidt Conference Abstracts,* Geochim. et Cosmochim. Acta 66/15A, 201; http://www.sediment.uni-goettingen.de/staff/dunkl/software/popshare.html

Frigo, C., Stalder, R., Hauzenberger, C.A., 2016. OH-defects in quartz in granitic systems

doped with spodumene, tourmaline and/or apatite: experimental investigations at 5-20 kbar. Physics and Chemistry of Minerals 43, 717-729.

Führing, P., 2017. Provenienz und Verteilung rezenter Sande der Nordseeküste (West- bis Ostfriesland) und der Flüsse Elbe, Weser und Ems. Unpublished MSc-thesis, University of Göttingen, 167 pp. (in German with English abstract)

Garzanti, E., Andò, S., Vezzoli, G., 2009. Grain-size dependence of sediment composition and environmental bias in provenance studies. Earth and Planetary Science Letters 277, 422-432.

Götze, J., Plötze, M., Habermann, D., 2001. Origin, spectral characteristics and practical applications of the cathodoluminescence (CL) of quartz – a review. Mineralogy and Petrology 71, 225-250.

Kats, A., 1962. Hydrogen in alpha quartz. Philips Research Reports 17, 133-279.

Le Heron, D.P., Meinhold, G., Bergig, K., 2013. Neoproterozoic–Devonian stratigraphic evolution of the eastern Murzuq Basin, Libya: a tale of tilting in the central Sahara. Basin Research 25, 52–73.

Lepper, J., Rambow, D., Röhling, H.G., 2013. Lithostratigraphie des Buntsandstein in Deutschland. Schriftenreihe der Deutschen Gesellschaft für Geowissenschaften 69, 69-149. (in German with English abstract)

Libowitzky, E., Rossman, G.R., 1997. An IR calibration for water in minerals. American Mineralogist 82, 1111-1115.

Malusà, M.G., Resentini, A., Garzanti, E., 2016. Hydraulic sorting and mineral fertility bias in detrital geochronology. Gondwana Research 31, 1-19.

Matter, A., Ramseyer, K., 1985. Cathodoluminescence microscopy as a tool for provenance studies of sandstones. In: Zuffa, G.G., (Ed.), Provenance of Arenite. Reidel Publishing Company, Dordrecht, Boston, pp. 191-211.

Meinhold, G., Morton, A.C., Avigad, D., 2013. New insights into peri-Gondwana paleogeography and the Gondwana super-fan system from detrital zircon U–Pb ages. Gondwana Research 23, 661-665.

Meinhold, G., Morton, A.C., Fanning, C.M., Frei, D., Howard, J.P., Phillips, R.J., Strogen, D., Whitham, A.G., 2011. Evidence from detrital zircons for recycling of Mesoproterozoic and Neoproterozoic crust recorded in Paleozoic and Mesozoic sandstones of southern Libya. Earth and Planetary Science Letters 312, 164-175.

Meyerink, T., von Eynatten, H., Dunkl, I., 2017. Late Permian to Early Triassic sediment provenance at the southeastern margin of the Central European Basin. Geo-Bremen, Abstract volume (https://www.dmg-home.org/fileadmin/Konferenzen/Abstracts_GeoBremen17.pdf), p.479.

Morton, A., Meinhold, G., Howard, J.P., Phillips, R.J., Strogen, D., Abutarruma, Y., Elgadry,

M., Thusu, B., Witham, A., 2011. A heavy mineral study of sandstones from the eastern Murzuq Basin, Libya: Constraints on provenance and stratigraphic correlation. Journal of African Earth Sciences 61, 308-330.

Müller, A., Knies, J., 2013. Trace elements and cathodoluminescence of detrital quartz in Arctic marine sediments – a new ice-rafted debris provenance proxy. Climate of the Past 9, 2615-2630.

Müller, A., Koch-Müller, M., 2009. Hydrogen speciation and trace element contents of igneous, hydrothermal and metamorphic quartz from Norway. Mineralogical Magazine 73, 569-583.

Ramos, E., Marzo, M., de Gilbert, J.M., Tawengi, K.S., Khoja, A.A., Bolatti, N.D., 2006. Stratigraphy and sedimentology of the Middle Ordovician Hawaz Formation (Murzuq Basin, Libya). AAPG Bulletin 90, 1309-1336.

Schade, J., 2018. Provenienzanalyse permo-triassischer Siliziklastika des Schwarzwalds. Unpublished MSc-thesis, University of Göttingen, 88 pp. (in German with English abstract)

Simon, T., Zedler, H., Müller-Schollenberger, V., 2013. Geologie und Hydrogeologie der Mineralwasserbohrung Ensingen. Jahreshefte Gesellschaft für Naturkunde Württemberg, Sonderband 2013, 147-228, Stuttgart. (in German)

Stalder, R., Konzett, J., 2012. OH-defects in quartz in the system quartz – albite – water and granite – water between 5 and 25 kbar. Physics and Chemistry of Minerals 39, 817-827.

Stalder, R., Neuser, R.D., 2013. OH-defects in detrital quartz grains: potential for application as tool for provenance analysis and overview over crustal average. Sedimentary Geology 294, 118-126.

Stalder, R., 2014. OH-defect content in detrital quartz grains as an archive for crystallization conditions. Sedimentary Geology 307, 1-6.

Stalder, R., Potrafke, A., Billström, K., Skogby, H., Meinhold, G., Gögele, C., Berberich, T., 2017. OH defects in quartz as monitor for igneous, metamorphic, and sedimentary processes. American Mineralogist 102, 1832-1842.

Table 1. Sample descriptions and OH contents

Figure captions:

Figure 1 Average IR spectra ($E||n_o$-$E||n_e$) of each sample. Bold spectra are scaled (according to the ratio of the average OH contents of the respective sample pair) in order to allow a better comparison of the band ratios of the two spectra of one succession. Spectra are normalised to 1 mm thickness and offset vertically for graphical reasons.

Figure 2 Histograms showing the OH defect contents in the analysed detrital quartz grains arranged in bins of 5 ppm. The black curve indicates a weighed distribution, taking into account an error of 2 wt ppm for each single data point > 2 ppm and 1 wt ppm for each data point < 2 ppm defect water. Average OH defect contents and number of measured grains are displayed in each plot.

Figure 3 Overview of the OH defect content of all samples as cumulative curves.

Figure 4 Component identification according to OH defect distribution for samples EY49-29 (A) and EY53-23 (B) assuming three OH defect components each (algorithm by Dunkl and Székely 2002): Results suggest the following component means, standard deviations (s.d.) and component percentages: (A) 0.6 ± 0.2 ppm (5%), 7.7 ± 4.8 ppm (66%) and 23.9 ± 8.5 ppm (29%), (B) 0.9 ± 1.1 ppm (39%), 4.6 ± 2.4 ppm (30%) and 18.2 ± 9.3 ppm (31%). For the model fitting all values below 1 ppm have been replaced by simulated values assuming normal distribution, mean of 0.5 ppm and s.d. of 1 ppm.

Figure 5 Decomposition of the OH defect distribution of the two Triassic samples assuming three potential sources, one OH poor source (only in EY54-11), one common intermediate source, and one OH rich source (only in EY54-18). Distribution of sample EY54-11 (sum of white and grey bars) and EY54-18 (sum of grey and black bars) results in a relative proportion of of 1:2:1, respectively. See Fig. 2 for comparison.

Table 1: Sample descriptions and OH-contents

	Sample	Sedimentation Period	Locality	Depth	Latitude	Longitude	N (grains)	OH content (wt ppm water) [1]		Reference
								average	range	
W5207	qtz-arenite	Cambrian	Central DEG/Libya		25°32.22' N	16°35.89' E	97	11	0-60	Morton et al. (2011)
H6048	qtz-arenite lithic	Ordovician	Central DEG/Libya		25°38.54' N	16°34.25' E	64	7	0-30	Morton et al. (2011)
EY54-18	subarkose lithic	Triassic (su-sm)	Ensingen/Germany	672.5 m	48°58.5' N	8°56.2' E	84	17	0-40	Schade (2018)
EY54-11	subarkose	Triassic (so)	Ensingen/Germany	426.0 m	48°58.5' N	8°56.2' E	128	9	0-45	Schade (2018)
EY49-29	river sand	recent	Torgau/Germany		51°33.1' N	13°01.2' E	88	12	0-45	Aschoff (2017)
EY53-23	river sand	recent	Geesthacht/Germany		53°25.2' N	10°16.2' E	82	8	0-65	Führing (2017)

[1] calculated using calibration of Libowitzky and Rossman (1997)
so = Upper Buntsandstein, sm = Middle Buntsandstein, su = Lower Buntsandstein

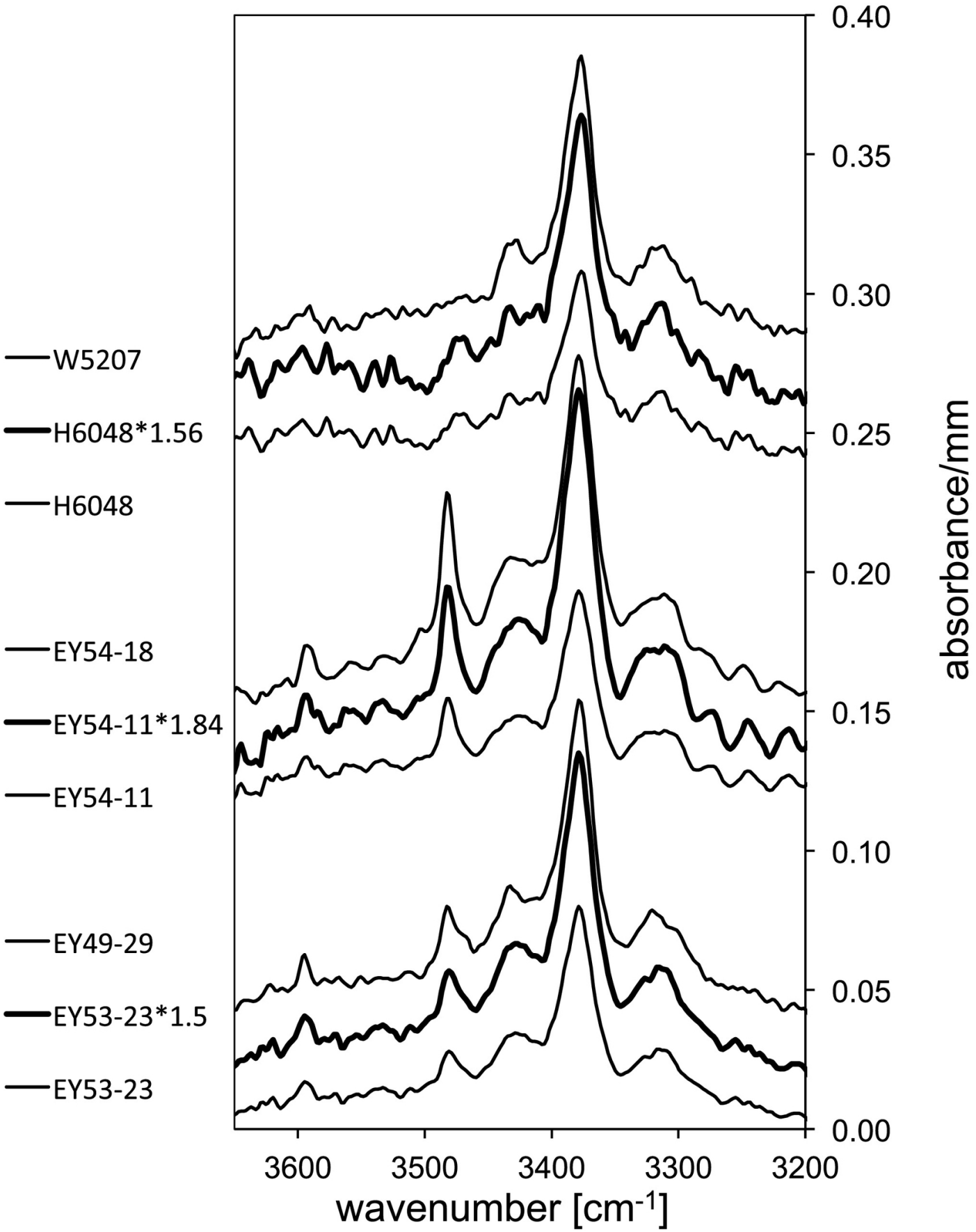
W5207
H6048*1.56
H6048
EY54-18
EY54-11*1.84
EY54-11
EY49-29
EY53-23*1.5
EY53-23
0.40
0.35
0.30
0.25
0.20
0.15
0.10
0.05
0.00
absorbance/mm
3600
3500
3400
3300
3200
wavenumber [cm-1]

Figure 1

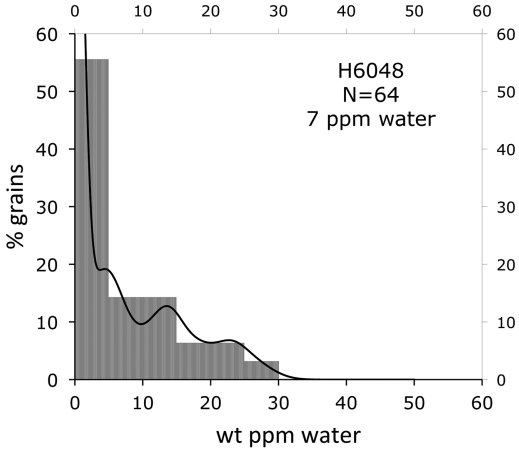
H6048
N=64
7 ppm water
% grains
wt ppm water

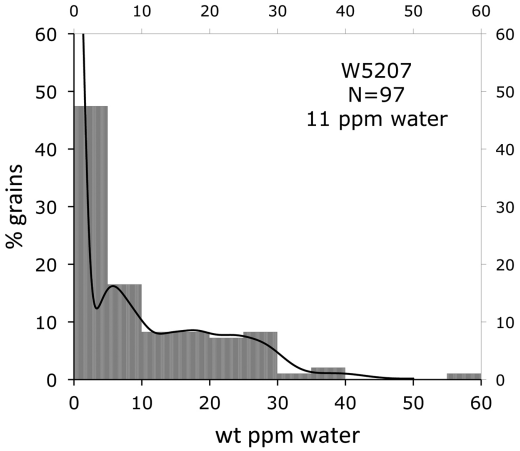
W5207
N=97
11 ppm water
% grains
wt ppm water

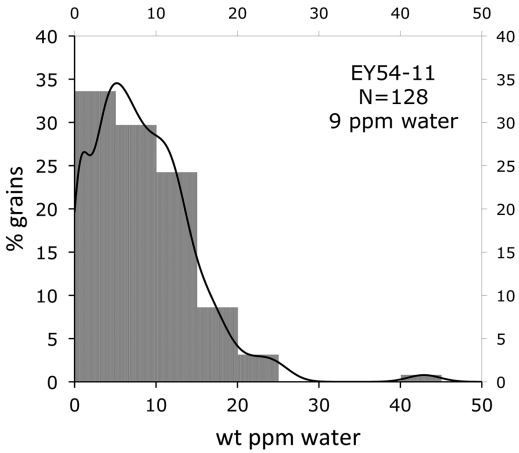
EY54-11
N=128
9 ppm water
% grains
wt ppm water

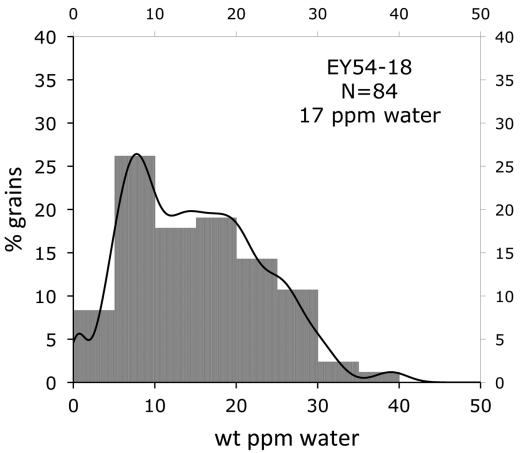
EY54-18
N=84
17 ppm water
% grains
wt ppm water

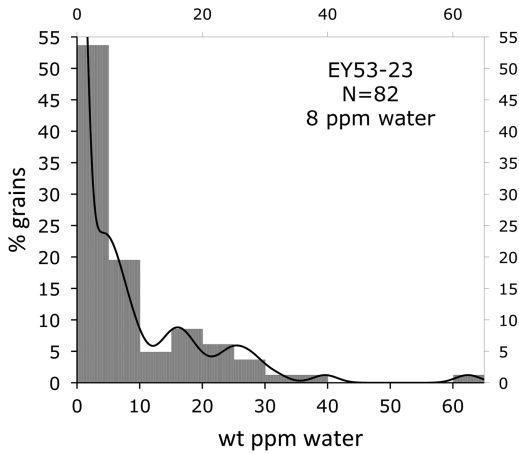
EY53-23
N=82
8 ppm water
% grains
wt ppm water

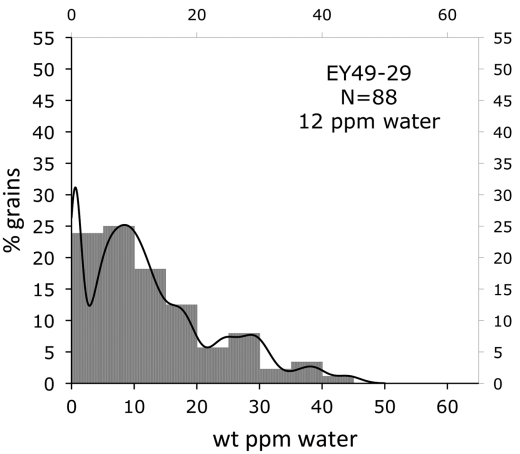
EY49-29
N=88
12 ppm water
% grains
wt ppm water

Figure 2

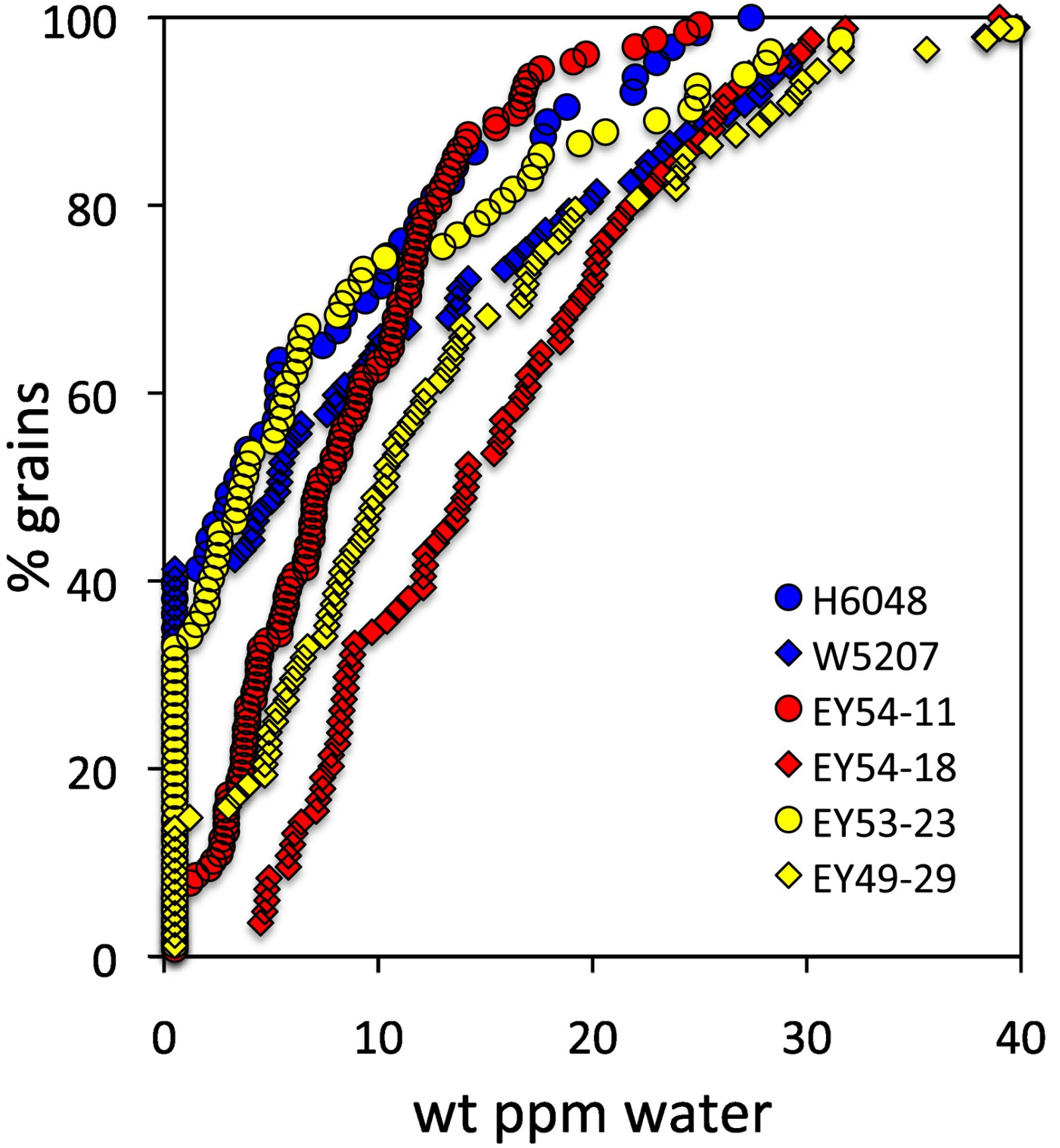
100
80
60
40
20
0
% grains
0
10
20
30
40
wt ppm water
H6048
W5207
EY54-11
EY54-18
EY53-23
EY49-29

Figure 3

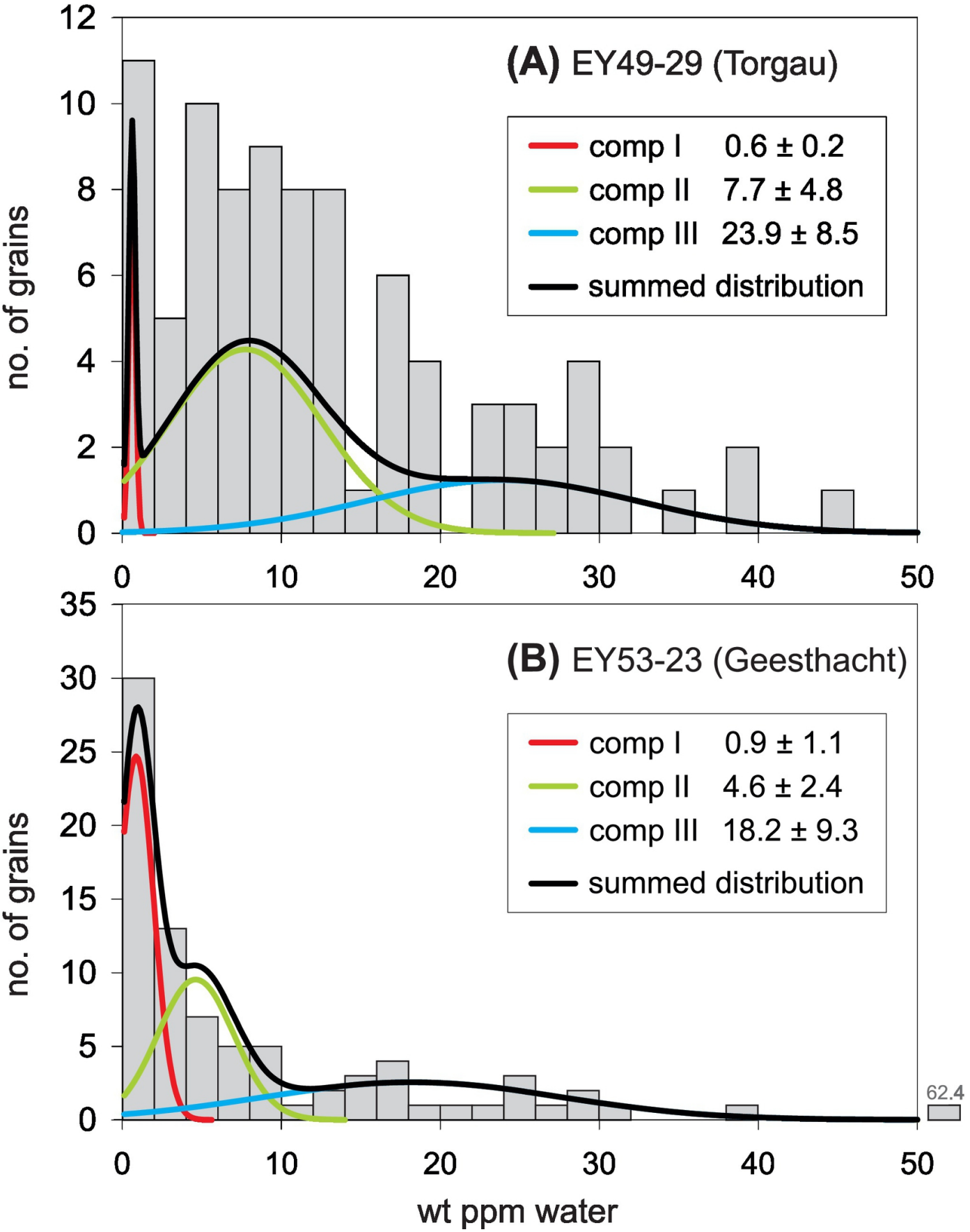
(A) EY49-29 (Torgau)
comp I 0.6 ± 0.2
comp II 7.7 ± 4.8
comp III 23.9 ± 8.5
summed distribution
no. of grains
(B) EY53-23 (Geesthacht)
comp I 0.9 ± 1.1
comp II 4.6 ± 2.4
comp III 18.2 ± 9.3
summed distribution
no. of grains
62.4
wt ppm water

Figure 4

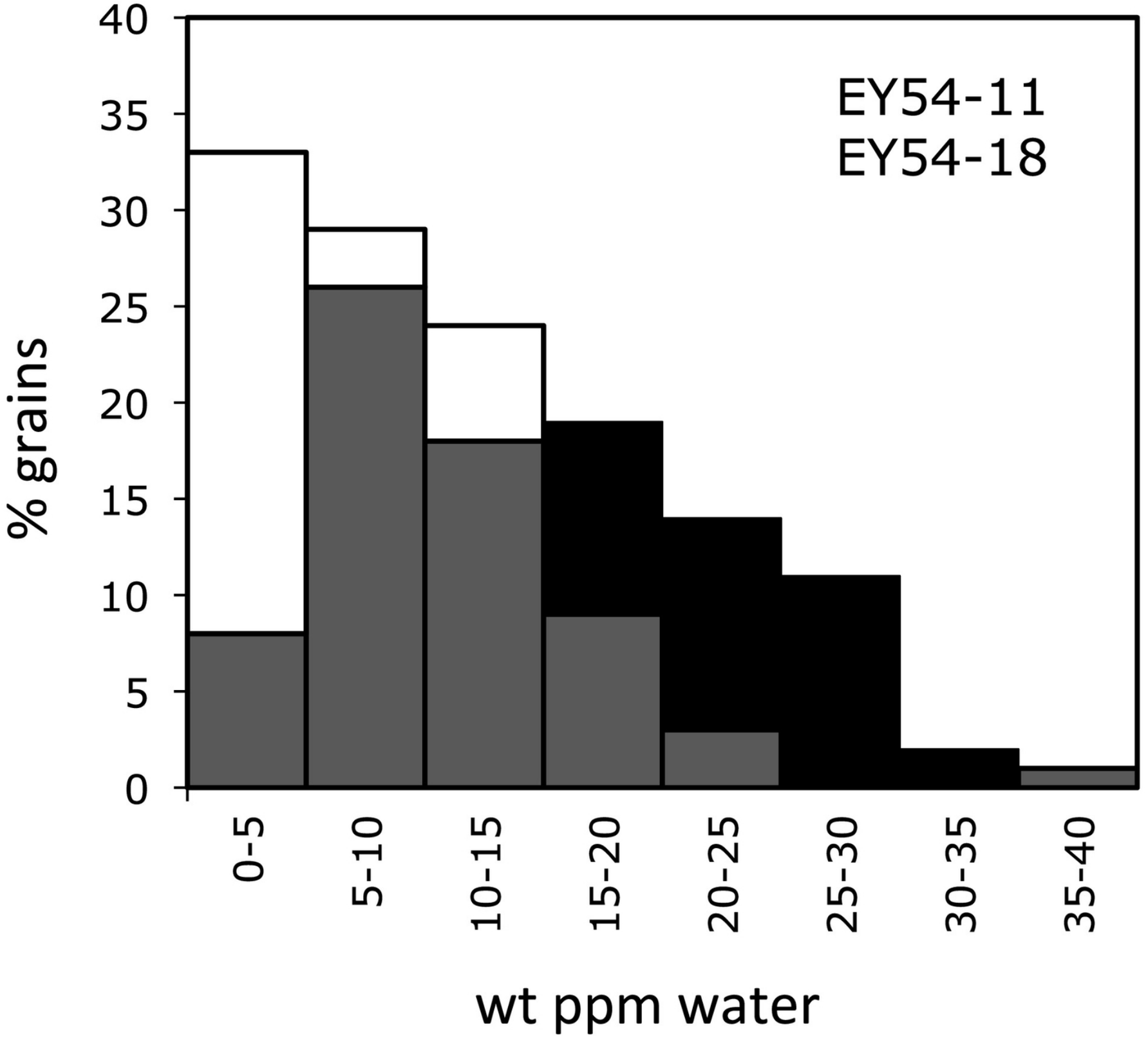
EY54-11
EY54-18
% grains
0
5
10
15
20
25
30
35
40
0-5
5-10
10-15
15-20
20-25
25-30
30-35
35-40
wt ppm water

Figure 5